CrossMark

Kinetics of the thermal degradation mechanisms in urea-formaldehyde cellulose composites filled with zinc particles

Muhammad Azeem Arshad[1] · AbdelKrim Maaroufi[1] · Rosario Benavente[2] ·
Gabriel Pinto[3]

Abstract This paper reports a study on the structural characterization, thermal stability, and thermal degradation kinetics of urea-formaldehyde cellulose (UFC) composites filled with zinc particles. Structural characterization of UFC/Zn composites carried out by SEM, XRD and FTIR analyses reveals that the composites are fairly homogenous, and the interactions between UFC and zinc in the composites are physical in nature. Afterwards, measurements of inherent thermal stabilities, probing reaction complexity, and thermal degradation kinetics of UFC/Zn composites have been carried out. The integral procedure decompositions temperature elucidates significantly higher thermal stabilities of UFC/Zn composites. Isoconversional kinetic analysis suggests multi-step reaction pathways of UFC/Zn composites in terms of the substantial variations in their activation energies with the reaction advancement. Advanced reaction model determination methodology with the help of an innovative kinetic function $F(\alpha, T)$ reveals that the thermal degradation of UFC goes to completion by following complicated multi-step nucleation/growth mechanisms. A detailed account of the mechanistic information regarding to the thermal degradation processes taking place
in UFC/Zn composites is given and discussed in the present study.

1 Introduction

Polymer composites containing zinc as filler are of great interest in an extensive range of global applications including, corrosion resistance, thermal/mechanical stability, electrical bi-stability, electromagnetic interference shielding, anti-microbial activity, etc [1–3]. The origin of this interest is actually the diverse fascinating properties of zinc like, non-poisonous, abundance and cheapness, light weight, good conductance and potential of exhibiting self passivity [4]. Loading zinc in urea-formaldehyde cellulose (UFC) matrix thus generates economical, environmentally friendly and multipurpose UFC/Zn composites [5]. Similar to other polymer/metal composites, UFC/Zn composites may either be electrically/thermally insulating or conducting though, both of them are equally useful. It is familiar that insulating composites are applicable as thermal greases, thermal interface materials, and electric cable insulations, while conductive composites are employable in thermoelectrical and thermomechanical applications, and organic electronics [6, 7].

Kinetic modeling of thermally stimulated condensed phase processes is capable of determining their activation parameters in order to analyze the transition states, and ultimately the process mechanisms. Kinetic parameters are physically meaningful in controlling the process under consideration for its eventual efficiency optimization, and predicting thermal stability/life of materials outside the experimental range. Nevertheless, thermally activated condensed phase processes are known for their complexities, and even an apparently simple reaction might consist of several steps.

✉ AbdelKrim Maaroufi
maaroufi@fsr.ac.ma; akarimmaaroufi@gmail.com

1 Laboratory of Composite Materials, Polymers and Environment, Department of Chemistry, Faculty of Sciences, University of Mohammed V, Ibn Batouta Avenue, P.O. Box 1014, Rabat, Morocco

2 Instituto de Ciencia y Tecnología de Polímeros (ICTP), Juan de la Cierva, 3, 28006 Madrid, Spain

3 Departamento de Ingeniería Química Industrial y del Medio Ambiente, E.T.S.I. Industriales, Universidad Politécnica de Madrid, 28006 Madrid, Spain

Authors have put forward an advanced approach to kinetically interpret the thermally stimulated condensed phase processes, and to cope with their complexities [8]. Thermal degradation behaviors of epoxy and epoxy/metal composites have already been simulated by the application of this approach, and profound insights into their thermal degradation pathways are obtained [9]. In the present research, the same approach will be applied to the thermal degradation of UFC/Zn composites, and the obtained mechanistic information will be interpreted and discussed.

2 Experimental

2.1 Formation of composites

Commercial grade urea-formaldehyde resin filled with α-cellulose, having 1.38 g cm^{-3} density and an electrical conductivity of around 1×10^{-13} S cm^{-1}, was supplied by Aicar S.A (Cerdanyola del Vallès, Spain). The total contents of α-cellulose contained by UFC resin were 30% by weight. The filler used was a commercial powder of zinc (Zn), delivered by Panreac (Castellar del Vallès, Spain) with about 96% purity, 7.14 g cm^{-3} density, 15 ± 10 μm average particle size, and an electrical conductivity of the order of 1.7×10^{5} S cm^{-1}. Both, the polymer and the metal powder were thoroughly dried at 60 °C for 48 h prior to use.

Zinc-filled UFC composites were prepared via blending and hot pressing route, by mixing the UFC matrix and zinc powder for 2 h in an especially designed internal mixer which operates with a rotation frequency of 60 revolutions per minute (rpm). The mixings were followed by compression molding in a specific mold with three cavities of 30.0 mm diameter and 3.0 mm thickness each one. The molding parameters were 20 MPa and 150 °C for 30 min. The freshly prepared samples were cooled at room temperature. In order to improve the finishing of pellet samples and for obtaining better structural characterization results, the surfaces of the samples were polished with sandpaper [5].

2.2 Scanning electron microscopy (SEM), X-ray diffraction (XRD) and fourier transform infrared (FTIR) analyses

In order to carry out the structural characterization and thermal analysis neat UFC and UFC/Zn composites, a pre-dried electrically insulator/conductor pair of composites was selected above and below the electrical percolation threshold (18.9 vol.% of zinc in UFC/Zn composites [5]) within the relatively stable conductivity regions and was named UFC/Zn5 and UFC/Zn37vol.%. respectively.

The homogeneity of UFC and UFC/Zn composites, their morphologies, and the dispersion of metallic particles inside the composite materials and polymer-metal interphases were analyzed by ultra high resolution cold field emission scanning electron microscope (UHR Cold-Emission FE-SEM SU8000) with accelerating voltages 2–3 kV. This instrument is fully computer-controlled and equipped with an EDX (energy dispersive X-ray) detector X-micro-analyzer.

X-ray diffraction analysis was carried out by X'pert Pro diffractometer in order to determine the number and types of internal phases present in UFC and UFC/Zn composites. Disk shaped samples were introduced into the diffractometer containing copper anode ($\lambda = 1.54$ Å), and the XRD analysis was performed within the Bragg angle $2\theta \in (3°, 90°)$.

Aiming to analyze the nature of bonding and interactions existing in pristine UFC and UFC/Zn composites, Fourier transform infrared (FTIR) analysis of UFC resin was carried out by employing attenuated total reflection (ATR) technique. For this purpose, FT/IR-4600 spectrometer was employed. The resin and the composites were scanned in transmission mode with a scanning rate of 2 mm sec^{-1} and resolution of 4 cm^{-1}, in the wave number range of 4000–500 cm^{-1}.

2.3 Thermogravimetric analysis

The thermoanalytical data of resin and composites were collected by Q500 V20.0 TGA analyzer which includes 100 μl aluminum pans, under non-isothermal experiment mode. For this purpose, samples of nearly similar geometries having masses 8–12 mg were employed, and the TG analysis was carried out in the range of heating rates, $\beta = 5$, 10, 15, and 20 °C min^{-1} from 30 to 600 °C under 90 ml min^{-1} nitrogen flow.

3 Theory

3.1 Kinetic analysis of thermally stimulated condensed phase processes

A thermally stimulated process is one in which the system needs to cross a potential energy barrier in order to shift itself from reactants to products. The energy distribution along the relevant coordinates in such a system is known to be governed by Boltzmann statistics. If the processes occurring in condensed phase are taken into consideration, several prominent physical phenomena and chemical reactions fall in this category. Physical phenomena include, vaporization and sublimation, glass transition and glass aging, nucleation, melting and crystallization of

polymers, solid–solid transition (for instance, ferromagnetic to paramagnetic transitions), etc. On the other hand, chemical reactions comprise; thermal decomposition of organic/inorganic materials, polymerization and cross linking reactions in polymers and thermal/thermo-oxidative degradation of polymeric materials [10–13]. Kinetic analysis of a thermally stimulated condensed phase process enables one to simulate the process rate by parameterizing generally the two variables i.e. degree of reaction advancement, denoted by 'α' and temperature 'T', by using the kinetic triplets which in turn, might probe into the process [12, 13]. In the case of polymeric and organic materials, although the differential scanning calorimetry may provide certain valuable information about the materials, though the assessment of their thermal degradation processes and particularly their kinetics are preferably carried out by thermogravimetric analysis (TGA) [14]. The unit-less parameter degree of reaction advancement or degree of conversion (α) of a thermally stimulated condensed phase process can be defined as following by employing thermogravimetric analysis:

$$\alpha = \frac{m_0 - m_t}{m_0 - m_\infty} \tag{1}$$

where, 'm_0' is the initial mass of reactant, 'm_t' is its mass at certain time 't' (isothermal TGA) or temperature (non-isothermal TGA) during the course of reaction and 'm_∞' is its mass at the end of reaction. In these processes, the reaction rate $d\alpha/dt$ being the function of 'α' can be represented as;

$$\frac{d\alpha}{dt} = kf(\alpha) \tag{2}$$

Equation (2) is the basic kinetic equation of solid state mass loss processes. In the case of thermally stimulated processes, the value of rate constant 'k' is often substituted in Eq. (2) by Arrhenius equation which then takes the following form;

$$\frac{d\alpha}{dt} = A \exp(-E_\alpha/RT)f(\alpha) \tag{3}$$

where, A is the pre-exponential factor, E_α is the energy of activation, $f(\alpha)$ is the function of degree of conversion, called reaction model, and R is gas constant. Physically, A describes the collision frequency of the particles involved in the formation of activated complex, E_α is the activation energy barrier of reaction, and $f(\alpha)$ is an expression for the mechanism of reaction [12]. Some well known condensed phase reaction models have been shown in Table 1 and graphically represented in Fig. 1.

Table 1 Well known reaction models of condensed phase processes

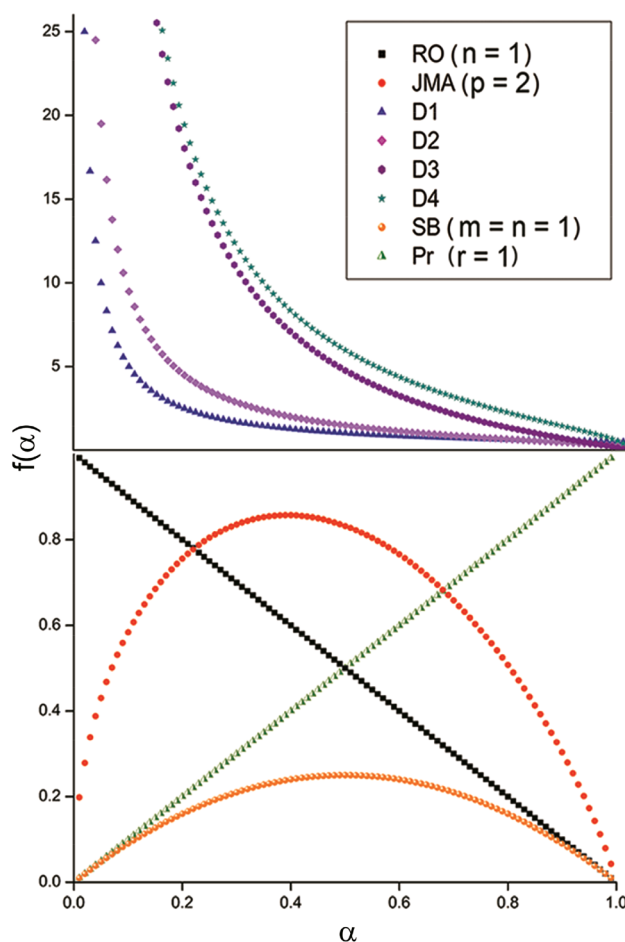| Reaction Model	Notation	$f(\alpha)$
Reaction order [15]	RO (n)	$(1-\alpha)n$
Johnson–Mehl–Avrami Equation [16]	JMA (m > 1)	$m(1-\alpha)\{-\ln(1-\alpha)\}^{1-1/m}$
1D-diffusion [17]	D1	$1/2\alpha$
2D-diffusion [18]	D2	$-1/ln(1-\alpha)$
3D-diffusion (Ginstling equation) [19]	D3	$\frac{3(1-\alpha)^{2/3}}{2\{1-(1-\alpha)^{1/3}\}}$
3D-diffusion (Jander's equation) [20]	D4	$\frac{3}{2\{(1-\alpha)^{-1/3}-1\}}$
Šesták-Berggren model [21]	SB (m, n)	$(\alpha)^m(1-\alpha)^n$
Power Law [22] (Nucleation)	Pr	$(\alpha)^r$

Fig. 1 Graphical representation of different cases of well known condensed phase reaction models

3.2 Determination of activation energy

Isoconversional methods are employed to examine the variation in activation energy with the degree of conversion (also called $E-\alpha$ dependency), and therefore the nature and complexity of process. A condensed phase process is fairly approximated as single step if the variation in its activation energy with the degree of conversion is insubstantial, otherwise, the reaction is perceived as obeying a complex reaction pathway. Isoconversional methods can be isothermal/non-isothermal, differential/integral and linear/nonlinear [13].

In the pursuance of determining reliable activation energies of condensed phase processes, a generalized linear integral isoconversional method (GLIM) has been suggested by Arshad and Maaroufi with the following mathematical expression [23]:

$$E_\alpha = \frac{R}{a}\left[b\frac{d\ln T_\alpha}{d(1/T_\alpha)} - \frac{d\ln\beta}{d(1/T_\alpha)}\right] \quad (4)$$

In Eq. (4), 'a' and 'b' are the constants which depend on temperature integral approximation [24]. For instance, $(a, b) = (1.052, 0)$ for Ozawa-Flynn-Wall (OFW) method [25]; $(a, b) = (1, 2)$ in the case of Kissinger-Akahira-Sunose (KAS) method [26], and $(a, b) = (1.0008, 1.92)$ in the case of Starink's method [27], etc. Moreover, in Eq. (4), $d\ln\beta/d(1/T_\alpha)$ and $d\ln T_\alpha/d(1/T_\alpha)$ respectively are the slopes of straight lines drawn between $\ln\beta$ and $1/T_\alpha$, and $\ln T_\alpha$ and $1/T_\alpha$ at certain value of α. The activation energy of a condensed phase process at any value of 'α' can be directly determined by employing Eq. (4), provided that the values of $d\ln\beta/d(1/T_\alpha)$ and $d\ln T_\alpha/d(1/T_\alpha)$ at the respective value of 'α' are known.

3.3 Determination of reaction model

Arshad and Maaroufi [23] have put forward an advanced reaction model determination methodology taking into account the variable activation energy concept in order to kinetically interpret the thermally activated condensed phase processes. The main advantage of this methodology is that it may not only simulate single step but also multi-step processes, and it is effectively applicable in isothermal as well as non-isothermal kinetics. In their approach, they avail a modified Arrhenius equation which includes variable pre-exponential factor and activation energy as described in Eq. (5):

$$\frac{d\alpha}{dt} = A_0(T/T_0)^n \exp(-E_\alpha/RT)f(\alpha) \quad (5)$$

where, 'A_0' is the value of pre-exponential factor at initial temperature 'T_0' and 'n' is a numerical constant. Usually $n \in [0, 1]$ but it may possibly attain positive values other than mentioned in the interval and it can even be a negative number.

On the basis of Eq. (5), authors have derived a new function of the degree of conversion $h(\alpha)$ to predict the reaction mechanisms of complex solid state processes [23]:

In the case of complicated reactions under non-isothermal conditions,

$$h(\alpha) = \frac{d^2\alpha/dt^2}{(d\alpha/dt)^2} + \frac{dE/d\alpha}{RT} - \frac{\beta\left\{n + \frac{E_\alpha}{RT}\right\}}{T(d\alpha/dt)} \quad (6)$$

In order to determine the parameter 'n' present in Eq. (6), Eq. (5) can be transformed into the following nonlinear form:

$$y = a(x)^b \exp(-c/x) \quad (7)$$

While, $x = T$, $y = d\alpha/dt$; $a = \varphi(\alpha) = \{A_0/(T_0)^n\}f(\alpha)$, $b = n$, $c = E_\alpha/R$.

As the reaction rate varies exponentially with temperature at constant values of 'α', the variation in reaction rate with temperature at constant values of 'α' can thus be fitted by an exponential type user defined fitting function (UDF) based on Eq. (7) employing Levenberg–Marquardt algorithm (LMA) for 2D curves, which ultimately results in the generation of parameters a, b and c.

It is worth pointing out that the accuracy of reaction model of a condensed phase process becomes sensitive to parameter 'n' when its activation energy acquires relatively lower value. However, when E_α/RT factor in Eq. (6) attains a value equal to or grater than 30 [28], the influence of parameter 'n' on the reaction model is generally insignificant, and Eq. (6) takes the following form:

$$h(\alpha) = \frac{d^2\alpha/dt^2}{(d\alpha/dt)^2} + \frac{1}{RT}\left[dE/d\alpha - \frac{\beta E_\alpha}{T(d\alpha/dt)}\right] \quad (8)$$

In both the discussed cases, the reaction model is evaluated by the following expression:

$$f(\alpha) = \exp\left(\int_0^1 h(\alpha)d\alpha\right) \quad (9)$$

A serious matter in the case of multi-step processes is related to identify the mechanisms of the individual reactions taking place within them. This trouble originates from the fact that only nucleation/growth models show peak functions and the rest of reaction models (if available in the reaction model curve) might not be visible in the

plots of $f(\alpha)$ by using Eq. (9) as evident in Fig. 1. In order to solve this issue, a new kinetic function $F(\alpha, T)$, taking into account the variation of reaction mechanism with temperature, is introduced in non-isothermal kinetics which is defined as:

$$F(\alpha, T) = \frac{df(\alpha)}{dT} = f'(\alpha)\frac{d\alpha}{dT} = \frac{1}{\beta}f'(\alpha)\frac{d\alpha}{dt} \qquad (10)$$

The obtained characteristic shapes of $F(\alpha, T)$ functions by applying Eq. (10) on the reaction models shown in Fig. 1, using an arbitrary single step reaction simulated by Runge–Kutta (RK4) method at 10 °C min^{-1}, are represented in Fig. 2. The activation energy and pre-exponential factor related to the simulated single step reaction are: E = 80 kJ mol^{-1} and A = 2×10^8 s^{-1}, respectively. It is anticipated that the developed $F(\alpha, T)$ function could be highly useful in identifying and distinguishing between various individual reaction mechanisms in a multi-step process.
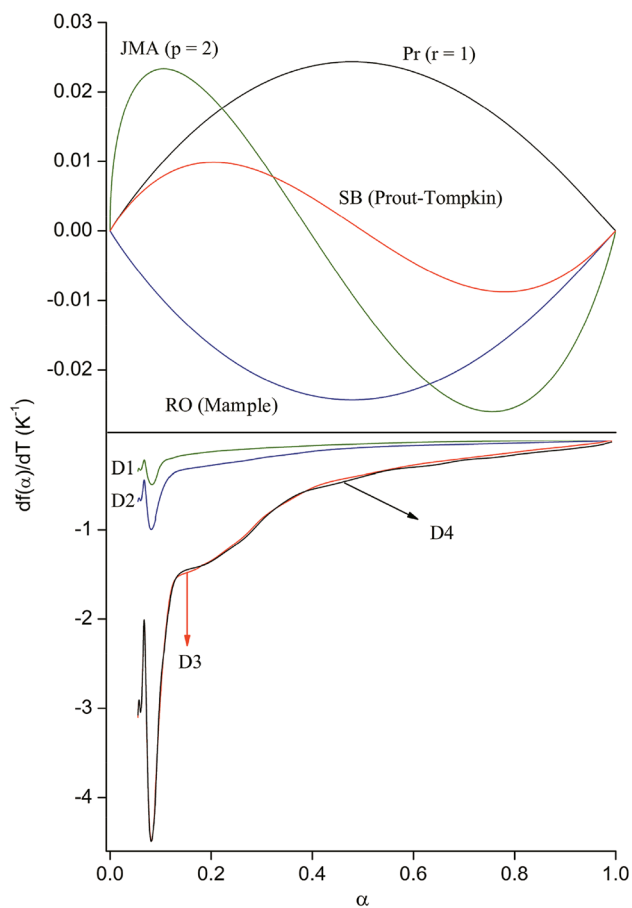

Fig. 2 Graphical representation of the application of new kinetic function F(α, T) = df(α)/dT on reaction models descried in Fig. 1, at 10 °C min^{-1}

4 Results and discussion

4.1 Structural characterization by SEM, XRD and FTIR analyses

The results obtained by performing cross sectional SEM analysis of pure UFC, UFC/Zn5vol.%, and UFC/Zn37vol.% composites, under the conditions described in "experimental" section, have been shown respectively in Fig. 3a–c. Different phases present in SEM micrographs can be identified by their differences in colors, contrasts, and the geometries of particles. SEM micrograph in Fig. 3a depicts that the resin is homogeneous, while SEM micrographs in Fig. 3b–c show the uniform distribution of zinc particles throughout the resin. The clusters of filler particles responsible for establishing infinite percolating network in conducting composite can also be visualized in Fig. 3c and its inset. Figure 3a–c also includes the EDX plots related to the scanning electron micrographs of pure UFC, UFC/ Zn5vol.% and UFC/Zn37vol.% composites. In all the cases, the intense peaks are due to the presence of carbon, nitrogen, oxygen, and zinc in the composites. Though the extremely low intensity peaks of aluminum and zinc in the EDX plot of pure UFC, and a common peak of sulfur in the EDX plots of pure UFC and UFC/Zn37vol.% composite, reveal their respective emergence as impurities in the resin and composite. It can be perceived on the basis of Fig. 3b–c that zinc might impart severe mechanical influence on UFC matrix, which results in damaging the resin chains available around zinc, and the development of stress by following micro-cracking mechanism. At higher loadings of zinc in UFC (UFC/Zn37vol.%), the sum of individual stresses can be able to introduce macro scale fractures in the composite structure, as evident in Fig. 3c. This behavior of UFC/Zn composites seems quite different from epoxy/Zn composite [6], though it is somewhat analogous to epoxy/Sn composites [9].

The results obtained by performing the X-ray diffraction of UFC and UFC/Zn composites, by following the conditions discussed in the "experimental" section, are presented in Fig. 4 in the diffraction angle 2-theta (2θ) ranging from 10° to 90°. It is obvious in the diffractogram of pure UFC in Fig. 4 that the internal structure of UFC is highly complicated due to the structural complexities of individual components and the interactions between them. Nine different peaks are observed and labeled as star symbol. Peaks existing at 14.17° and 15.35° are the overlapped peaks which define crystalline phases present in cellulose [29]. Partially overlapped geminal peaks available at 20.56° and 21.96° can be allocated respectively to the crystalline phase present in urea-formaldehyde, [30, 31] and the amorphicity of cellulose [29]. Peaks existing around 26° and 30° are also typical peaks of urea-formaldehyde [30, 31]. Three sharp
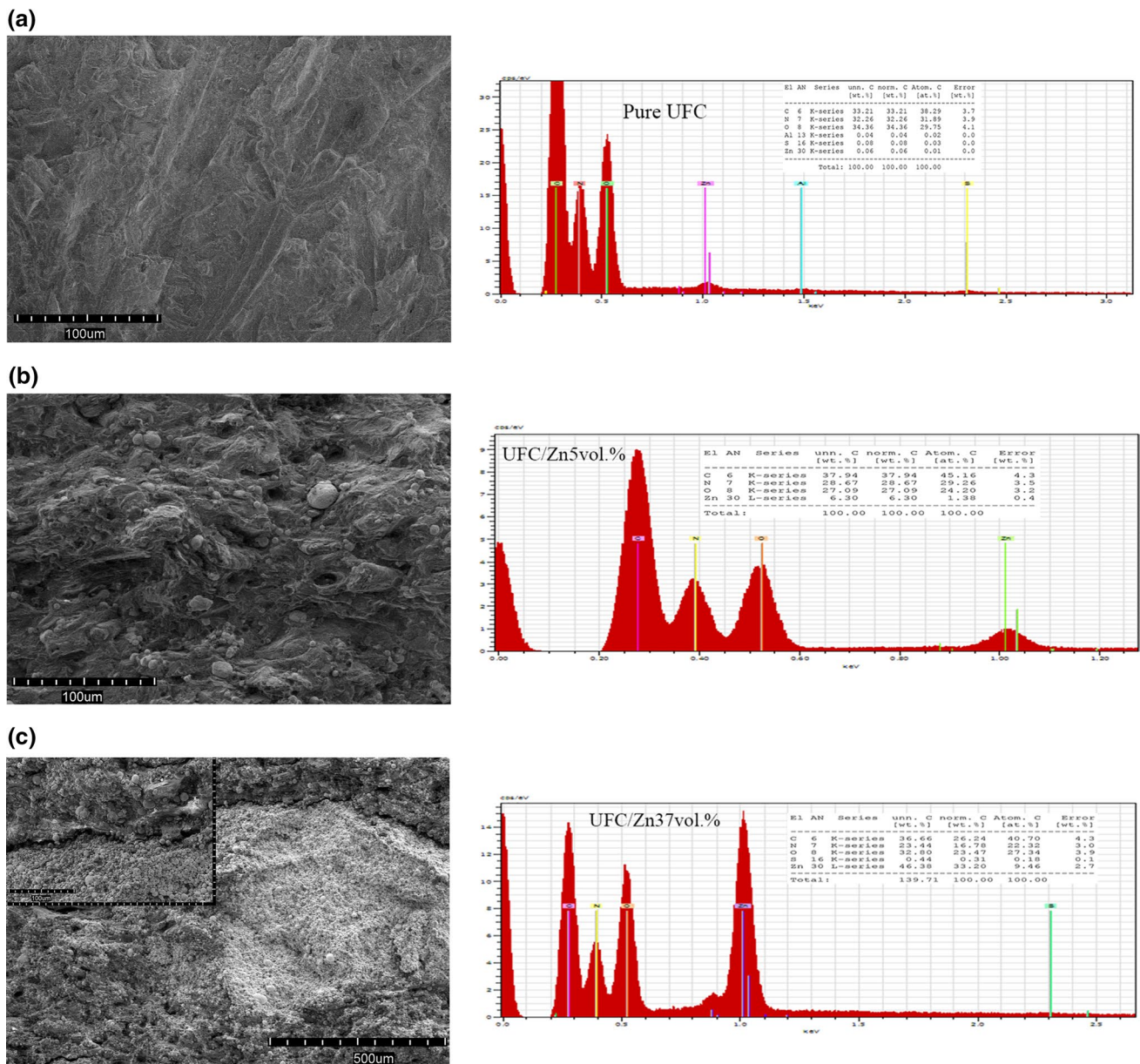
(a)

(b)

(c)

Fig. 3 Cross-sectional scanning electron micrographs of **a** pure UFC, **b** UFC/Zn5vol.% and **c** UFC/Zn37vol.% along with their respective EDX plots

but relatively low intensity peaks at 47.34°, 51.54° and 56.19° appear as a result of the hydrogen bond formation between urea-formaldehyde and cellulose as elaborated in the previous study [32].

In the case of UFC/Zn composites, the diffractograms in Fig. 4 show additional peaks at 36.25°, 38.98°, 43.18°, 54.27°, 70°, 70.62°, 76.95°, 78.9°, 82.01°, 83.71°, and 86.48°. Peaks available at 6.25°, 38.98°, 43.18°, 54.27°, 70°, 70.62°, 76.95°, 82.01°, 83.71°, and 86.48° and labeled as inverted triangle symbol in Fig. 4 can be assigned to Zn/ZnO (due to partial oxidation of filler [33]). The information regarding the peak positions of Zn/ZnO in Fig. 4

agrees with that obtained from Joint Committee on Powder Diffraction Standards: The International Centre for Diffraction Data (JCPDS-ICDD) card for pure Zn (JCPDS-ICDD PDF #00-004-0831) [34] and ZnO (JCPDS-ICDD 036-1451) [34], confirming the presence of principal crystalline hexagonal close-packed (hcp) phase of Zn and partial crystalline hexagonal wurtzite phase of ZnO in the composites. The Peak existing at 78.92° and labeled as square symbol in Fig. 4 can be attributed to wurtzite phases of ZnS present in the filler as impurity. The presence of sulfur as impurity in composites has already been pointed out in the EDX plot of UFC/Zn37vol.% in Fig. 3d. Moreover, though

Fig. 4 X-ray diffractograms of pure UFC, UFC/Zn5vol.%, and UFC/Zn37vol.%. The peak positions of filler (Zn) in composites show conformity with the Joint Committee on Powder Diffraction Standards: The International Centre for Diffraction Data (JCPDS-ICDD) card for pure Zn (JCPDS-ICDD PDF #00-004-0831) [34]
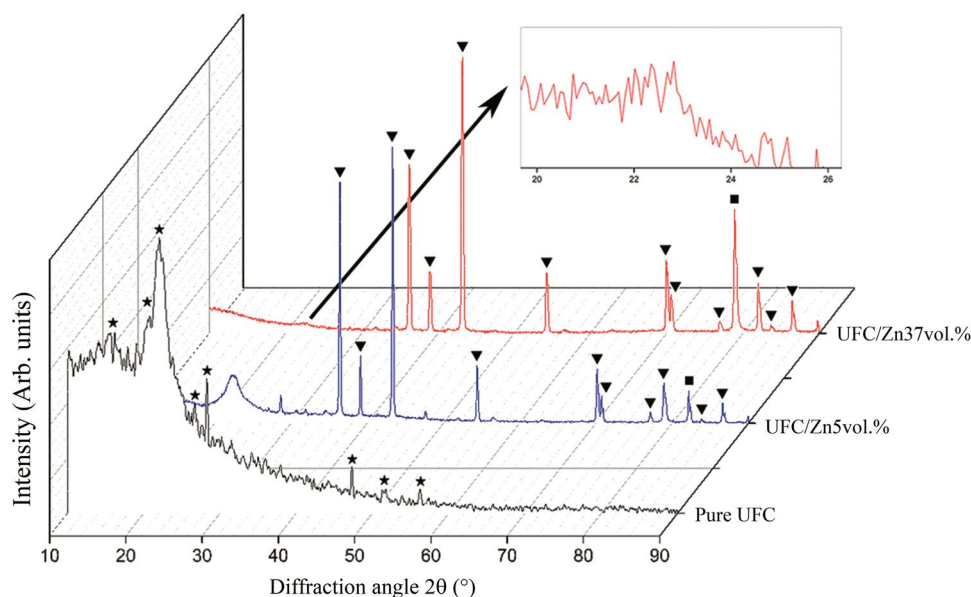
the peak intensities relevant to organic phases substantially reduce by enhancing zinc contents in composites, yet the individual components of composites retain their identities in composites (see for instance, inset of UFC/Zn37vol.% diffractogram).

The results obtained by carrying out FTIR-ATR analysis of UFC and UFC/Zn composites, by following the conditions given in the "experimental" section, are demonstrated in Fig. 5. A significantly broad band ranging around 3650–3000 cm^{-1} is a convoluted band as both urea-formaldehyde and cellulose absorb in this region. It consists of a peak available around 3350–3450 cm^{-1} that can be attributed to the hydrogen bonded O–H and N–H, and its broadness might be due to the presence of water and formaldehyde. The O–H groups of water and formaldehyde of urea-formaldehyde may potentially form hydrogen bonds with reactive functional groups such as CH_2OH, NH_2 and NH [35]. This convoluted band also includes a peak at 3337 cm^{-1} corresponding to OH stretching, and is associated with the intramolecular hydrogen bonds of cellulose [36]. However, the convolution of the two mentioned peaks results in a broad peak at relatively lower wave number (3300 cm^{-1}) in UFC due to the interactions between urea-formaldehyde and cellulose, which more likely lead to the formation of hydrogen bonds between them, as detailed in the previous study [32]. The two small bands at 2920 and 2850 cm^{-1} are typical of the C–H and O–H stretching vibrations of cellulose/hemi-cellulose and lignin, respectively [37], elucidating that the cellulose is of plant origin. Two overlapped peaks at 1627 and 1527 cm^{-1} respectively are attributable to –N–H bending vibrations of amide II (secondary). The peak of relatively low intensity at 1375 can be assigned to the stretching C–N vibrations
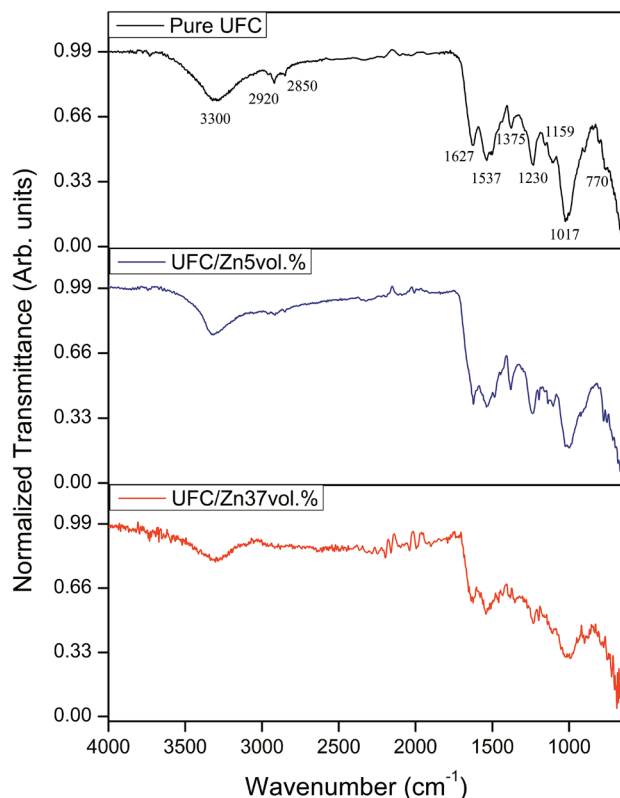

Fig. 5 FTIR spectra of pure UFC, UFC/Zn5vol.% and UFC/Zn37vol.%

of amide I & II (primary and secondary), while it has also been assigned to C–H stretching and –O–H bending vibrations of alcohol [38]. The peak at 1230 cm^{-1} is assigned to C–N stretching vibrations of amide II [39]. A peak of very

low intensity at 1159 cm^{-1} is ascribed to both the asymmetric stretches of N–CH$_2$–N and –C–O–C– of ether linkages [40]. A strong and broad peak at 1017 cm^{-1} is due to C–C–O stretching of CH$_2$OH, and an extremely weak peak at 770 cm^{-1} (which is relatively more prominent in the case of composites) is ascribed to –N–H bending and wagging vibrations of amide I & II [38]. Figure 5 also shows the FTIR spectra of UFC/Zn composites. The FTIR spectra of UFC/Zn composites seem analogous to each other and to that of pure UFC (neglecting the noise in FTIR spectrum of UFC/Zn37vol.%) which corroborates the information obtained by SEM and XRD analyses. The reduction in the peak intensities in the case of UFC/Zn37vol.% is although due to decrease in relative proportion of UFC in the conducting composite, as been pointed out in XRD of UFC/Zn37vol.% composite.

The consistent information obtained by SEM, XRD and FTIR analyses shows that the resin and composites are fairly homogeneous, and that the interactions existing between UFC and zinc in composites could possibly be of physical nature.

4.2 Thermal degradation of UFC and UFC/Zn composites

The percentage mass loss and normalized DTG curves of UFC and UFC/Zn composites as the functions of temperature, under the experimental conditions described in TGA measurements section are shown in Fig. 6a–c respectively. The nature of degradation process is determined by shape/position of TGA/DTA curve and it is strongly dependent on the material's constituents. Thermal degradation of UFC seems a complex process as can be visualized in Fig. 6a. Apparent reaction profile of UFC, as evidenced by TG/DTG curves in Fig. 6a, identifies the occurrence of various reactions over long temperature range. It has already been shown that the thermal degradation of UFC resin goes to completion by following at least four steps [32]. The first step which ranges between 50 to 215 °C may involve mainly the dehydration of resin, and partly the scission of weaker intermolecular/intramolecular linkages like, hydrogen bonding, polymer–polymer interactions, etc. The second step occurring between 220 and 275 °C could be the conversion of methyl ether functional groups of UFC into methylene functional groups and branching/cross linking reactions which probably shifts to somewhat higher temperatures due to the presence of interactions between urea-formaldehyde and cellulose [30, 32, 40, 41]. The third step is available between 280 to 350 °C with substantial mass loss and broad DTG peak which may consist of several processes. In this temperature range, the main reactions are: participation of the radicals formed by chain scission into formation of polymeric cyclic structures, formation of
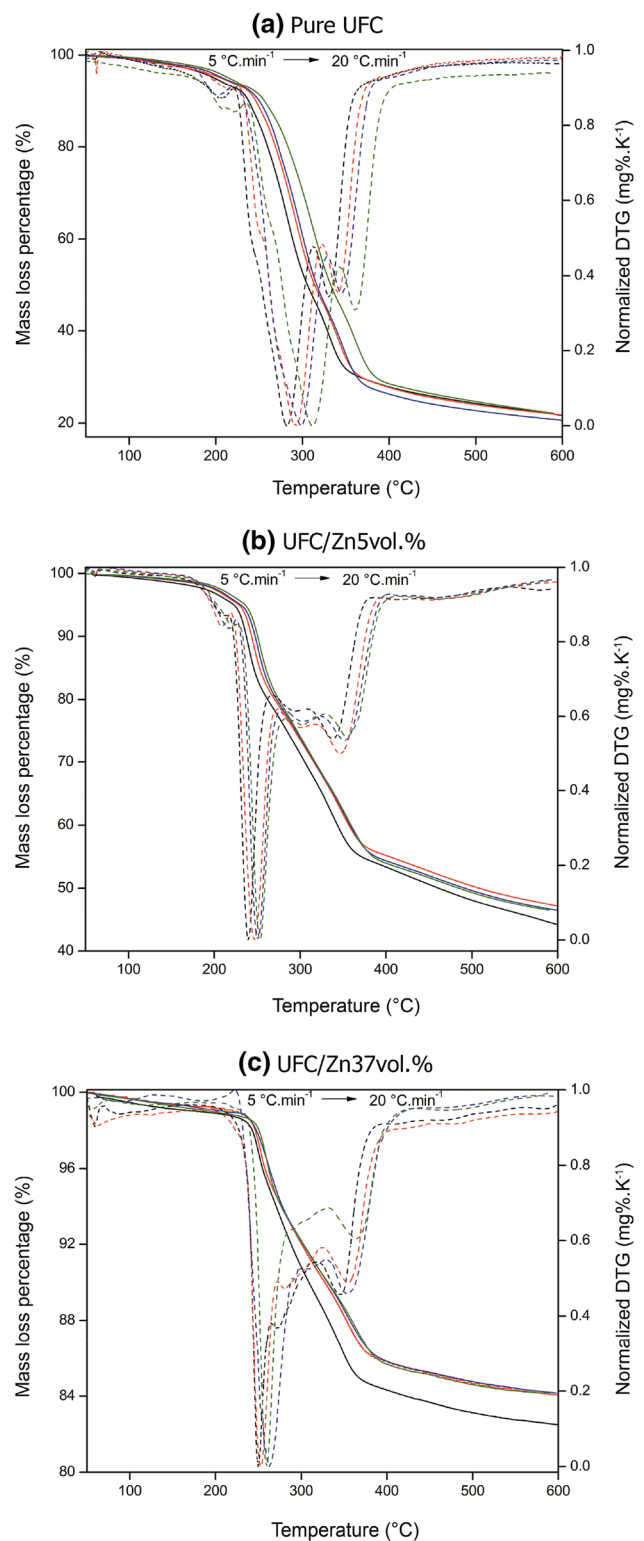

Fig. 6 TG/DTG curves at different heating rates of **a** pure UFC, **b** UFC/Zn5vol.% and **c** UFC/Zn37vol.%

active cellulose which is associated to the scission of glycosidic bonds and the dehydration of pyranose rings, producing anhydrocellulose, CO_2, volatile gases and unsaturated cyclic compounds [42–45]. The final step responsible for the rest of the mass loss takes place above 350 °C, and is associated with char formation. Since TG curves shift to higher temperatures with the increase in heating rate, therefore, common thermal degradation temperature ranges related to various reaction steps have been chosen by taking into account all the employed hating rates.

Figure 6b–c shows the thermal degradation behaviors of UFC/Zn composites. According to Fig. 6b–c, the thermal degradation behaviors of UFC/Zn composites seem, up to certain extent, similar to UFC resin. Nevertheless, the intensity of DTG peak related to the second thermal degradation step in the case of conducting composite is considerably reduced, and this intensity reduction is remarkable particularly at higher heating rates as can be seen in Fig. 6c. Similar phenomenon has already been pointed out in the case of UFC/Al composites [46]. Figure 7 shows the comparison of TG/DTG curves of pure UFC, UFC/Zn5vol.% and UFC/Zn37vol.% at 20 °C min⁻¹ heating rate. Figure 7a represents that overall, zinc is capable of providing substantial shield against the thermal degradation of UFC, and the increase in thermal stability of UFC resin depends on the contents of zinc in UFC. Actually, thermal degradation behaviors shown by UFC/Zn composites in Fig. 7a are entirely apparent, as the TG curves in Fig. 7a include also the mass of zinc, called uncorrected TG curves. In order to find the true effect of zinc on UFC resin, the mass of zinc is subtracted from the apparent masses of composites pair at each temperature at 20 °C min⁻¹, and the TG curve of UFC along with the corrected TG curves of UFC/Zn composites are drawn versus temperature, as given in Fig. 7b. A comparison between Fig. 7a, b demonstrates that the actual effect of zinc on the thermal degradation of UFC resin is irregular, and it is dependent on zinc contents in UFC. Particularly, the third reaction step shifts to lower temperatures which is evident from temperatures of UFC and UFC/Zn composites at maximum reaction rates (T_{max}.) i.e. $(T_{max}.)_{UFC} = 311.52$ °C; $(T_{max}.)_{UFC/Zn5vol.\%} = 252.88$ °C; and $(T_{max}.)_{UFC/Zn37vol.\%} = 260.08$ °C. In addition, this reaction step (more probably catalyzed by zinc contents) shows potentially different reaction pathway, and the degradation reactions in composite systems seem to be transformed from competitive to successive. It has already been explained in detail in the previous studies [6, 9, 47] that the competing variations in catalytic activities and heat capacities of metals with temperature are among the major factors which may define the thermal degradation behaviors of polymer/metal composites. In this regard, the principle reason behind the thermal degradation behavior shown by UFC/Zn composites, on one hand, can be its fine catalytic
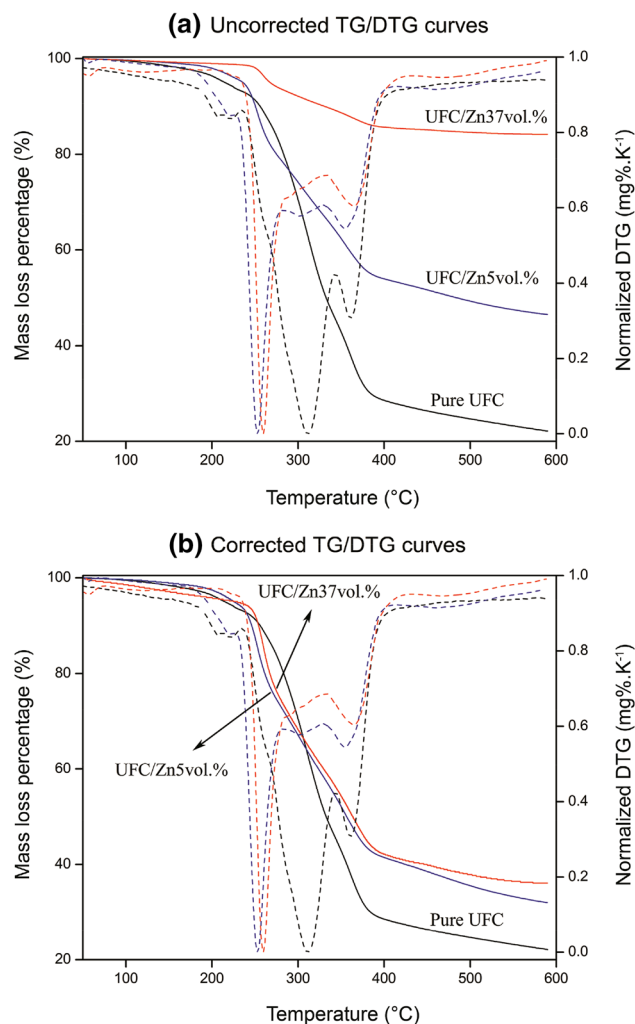

Fig. 7 **a** Uncorrected TG/DTG curves of UFC/Zn5vol.% and UFC/Zn37vol.%, **b** Corrected TG/DTG curves of UFC/Zn5vol.% and UFC/Zn37vol.%, at 20 °C min⁻¹

activity at ordinary temperatures and catalytic deactivation at higher temperatures [48]. While on the other hand, the heat capacity of zinc exhibits absolutely converse behavior with temperature (0.39 J g⁻¹ K⁻¹ to 0.51 J g⁻¹ K⁻¹ as temperature changes from standard to melting point of zinc i.e. 419.5 °C) rendering the thermal stability of composites to augment, especially at higher filler loadings. It is worth remarking that the thermal degradation behaviors manifested by UFC/Zn composites are however quite different than epoxy/Zn composites [6]. Such comparison enables us to perceive that the thermal degradation behavior of insulating/conducting polymer/Zn composites might not only be affected by temperature dependence of physical properties of zinc but also by the nature of polymer (structure and properties) and its individual thermal degradation behavior over long temperature ranges.

Thermal stability of UFC resin and the influence of zinc contents on the thermal stability of UFC can be evaluated by various parameters including initial decomposition temperature (T_i), temperature at maximum reaction rate (T_m), final decomposition temperature (T_f), and statistic heat-resistant index (T_s) [49]. Although, an efficacious and physically more meaningful parameter called integral procedure decomposition temperature (IPDT), is usually employed to estimate the inherent thermal stabilities of polymer/polymer composites [50, 51]. IPDT correlates the volatile parts of polymers/polymer composites and is expressed by the following equation:

$$IPDT(^\circ C) = T_i + A^* K^* (T_f - T_i) \qquad (11)$$

where,

$$A^* = \frac{A_b + A_c}{A_a + A_b + A_c} \qquad (12)$$

$$K^* = 1 + \frac{A_c}{A_b} \qquad (13)$$

In Eq. (11), T_i is the initial decomposition temperature of polymer (usually corresponds to 5% mass loss), T_f is the final decomposition temperature, and A^* and K^* are constants which can be calculated by Eqs. (12), (13). In Eqs. (12), (13), A_a and A_b respectively are the areas above and below the TG thermogram, while, A_c is the complementary area of oblong rectangle as already been elaborated [9].

By employing Eqs. (11)–(13) and following the procedure discussed above, the IPDT values of pure UFC and UFC/Zn composites for both the uncorrected and corrected TG curves at 20 °C min^{-1} have been calculated and shown in Table 2. The calculated IDPT value of UFC resin is 547 °C which shows its higher thermal stability comparative to epoxy resin with IPDT value 478 °C under similar experimental conditions [9]. The IPDT data obtained from uncorrected TG curves of UFC/Zn composites show significantly higher thermal stabilities of these composites. However, the actual thermal stabilities obtained by corrected TG curves of UFC/Zn composites are relatively less.

Table 2 Integral procedure decomposition temperature (IPDT) values in the case of uncorrected and corrected TG curves of pure UFC and UFC/Zn composites at 20 °C min^{-1}

Sample	IPDT (°C) of uncorrected TG curves	IPDT (°C) of corrected TG curves
Pure UFC	547	–
UFC/Zn5vol.%	695	610
UFC/Zn37vol.%	847	634

Despite the discussed, the IPDT results in Table 2 demonstrate that the overall influence of zinc on UFC is providing thermal stability to matrix and this thermal stabilization effect seems the function of zinc contents in UFC/Zn composites. These results are evidently contrary to epoxy/Zn composites [6].

On the basis of the above discussion and IPDT values of pure UFC and UFC/Zn composites, it is inferable that the influence of zinc on the thermal degradation of UFC is non-uniform, and it might predominantly be governed by the net effect of competitive temperature dependent variations in catalytic activity and heat capacity of zinc, zinc contents in composites, and the structure and thermal degradation behavior of matrix itself. In this frame of reference, it has been found that zinc is capable of considerably enhancing the thermal stability of UFC resin, and the thermal stability of resin seems directly related to quantity of zinc in UFC/Zn composites.

4.3 Thermal degradation kinetics of UFC and UFC/Zn composites

Kinetic analysis on the thermoanalytical data of UFC and UFC/Zn composites can help in profound understanding and detailed interpretation of their discussed thermal degradation behaviors. In the present study, generalized linear isoconversional method (GLIM) as mathematically expressed in Eq. (4) within $\alpha \in [0.05, 0.95]$ has been applied on the thermoanalytical data of UFC and UFC/Zn composites by exploiting a relatively more accurate temperature integral approximation suggested by Starink [27]. Figure 8a–c shows the results obtained by the application of GLIM on pure UFC, UFC/Zn5vol.% and UFC/Zn37vol.%, respectively. In all the cases, the straight lines are linear at each degree of conversion value chosen and therefore the activation energy values are reliable. Figure 9 represents the comparison of variation in activation energy with the degree of conversion obtained by isoconversional analysis of pure UFC, UFC/Zn5vol.% and UFC/Zn37vol.%, respectively, along with the uncertainty bars.

4.3.1 $E - \alpha$ dependencies interpretations of UFC and UFC/Zn composites

The reaction profiles of UFC and UFC/Zn composites are evidently multiplex, and they fall among the examples of complicated condensed phase processes. Four different regions can be marked in Fig. 9 which represents the $E - \alpha$ dependency patterns of UFC and UFC/Zn composites obtained by GLIM. These regions are consistent with the already discussed thermal degradation behaviors of UFC and UFC/Zn composites in the previous section. The effective activation energies in these regions have been shown
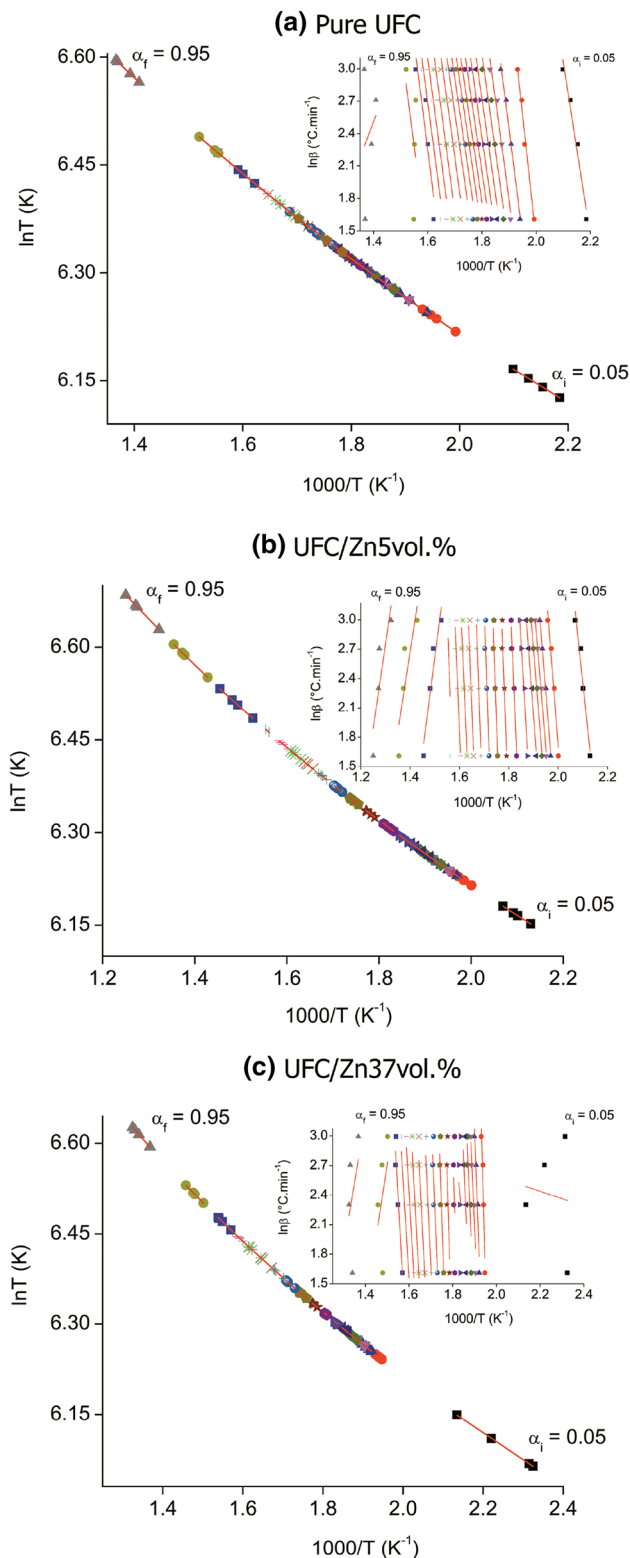
(a) Pure UFC

(b) UFC/Zn5vol.%

(c) UFC/Zn37vol.%

Fig. 8 Application of generalized linear integral isoconversional method (GLIM) on non-isothermal degradation of **a** pure UFC, **b** UFC/Zn5vol.% and **c** UFC/Zn37vol.%
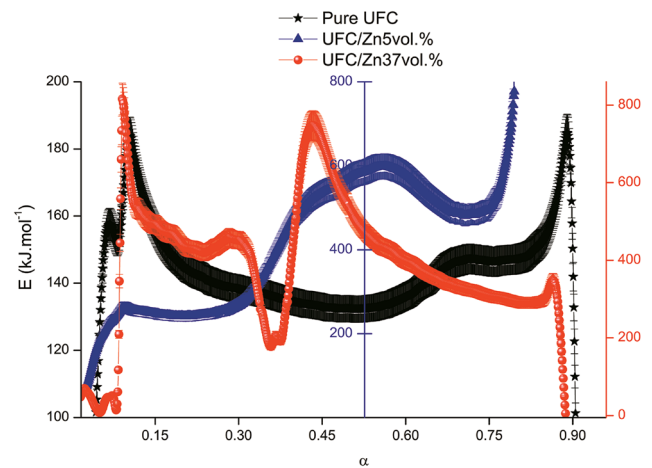

Fig. 9 Comparison of the variations in thermal degradation activation energies with the degree of conversion between pure UFC, UFC/Zn5vol.% and UFC/Zn37vol.%

in Table 3. In the case of E−α dependency of UFC, the first region corresponds to (0, 0.065) of α giving information about initial mass loss that could predominantly be due to the dehydration of resin and/or some weaker interactions present in the macromolecular structure of resin. The effective E_α value in this region is 99 kJ mol^{-1} which seems reasonable as the dehydration energy remains generally between 60 and 100 kJ mol^{-1}. The second region ranges between (0.065, 0.4) of α with an effective value of 147 kJ mol^{-1} that might be assigned to the conversion of methyl ether functional groups into methylene functional groups and branching/cross linking reactions. The third region is associated with (0.4, 0.8) of α, and comprises competitive principle degradation reactions of UFC resin. Activation energy shows considerable variations in this region due to the involvement of various reactions. 139 kJ mol^{-1} is the effective energy of reactions found in this region. The fourth and the last region is related to [0.8, 1] of α. The activation energy of fourth step is mainly ascribed to char formation. It is noticeable that the values of E_α are unstable ahead α = 0.9, therefore, an average value of activation energy 159 kJ mol^{-1} in the interval [0.8, 0.9] has been taken.

In the case of UFC/Zn composites, obtained E-α dependencies demonstrate quite different behaviors of variation of activation energy with the degree of conversion in comparison with UFC resin. It probably means that the UFC/Zn composites follow different thermal degradation mechanisms than UFC resin and this alteration possibly depends on the contents of zinc in UFC/Zn composites. The degree of conversion intervals of 1st and 2nd thermal degradation steps of UFC/Zn composites are the same as in UFC resin. However, the degree of conversion intervals of 3rd and 4th thermal degradation steps of UFC/Zn composites

Table 3 Effective activation energy values of individual reaction steps in multi-step thermal degradation of UFC and UFC/Zn composites, determined by generalized linear integral isoconversional method (GLIM)

Sample	E_{Step1} (kJ mol^{-1})	E_{Step2} (kJ mol^{-1})	E_{Step3} (kJ mol^{-1})	E_{Step4} (kJ mol^{-1})
Pure UFC	99 ± 10	147 ± 4	139 ± 10	159 ± 17
UFC/Zn5vol.%	101 ± 7	281 ± 7	558 ± 13	526 ± 15
UFC/Zn37vol.%	39 ± 10	405 ± 15	514 ± 20	314 ± 10

have been chosen respectively as (0.4, 0.65) and (0.65, 0.85). The reason behind these selections is that the thermally activated processes in the third degradation step of UFC/Zn composites shift to lower temperatures, and ahead $\alpha = 0.85$, activation energy values are highly scattered (and therefore unreliable) due to extremely slow and noisy reaction rate. On the basis of Fig. 9 and Table 3, it might be stated that the higher activation energies of principle degradation steps of UFC/Zn composites substantially contribute in enhancing their thermal stabilities. These results do not agree with those obtained from epoxy/Zn composites [6].

4.3.2 Reaction models and thermal degradation mechanisms of UFC and UFC/Zn composites

Prediction of reaction mechanism is the eventual aim of a kinetic study, and it is considered as one of the most important applications of reaction kinetics. Substantial variations in the activation energies of UFC and UFC/Zn composites verify multi-step nature of their thermal degradation. The calculated value of E_α/RT factor over the whole domain of conversion degree shows that this factor remains always equal or greater than 30 for UFC and UFC/Zn composites, making the use of Eq. (8) appropriate for these materials.

Therefore, normalized curves of reaction models and their variations with temperature i.e. $f(\alpha)$ and df/dT respectively, as determined by applying Eqs. (8)–(10) on the thermoanalytical data of UFC and UFC/Zn composites at 20 °C min^{-1}, are shown in Fig. 10. Figure 10 clearly suggests that thermal degradation of UFC and UFC/Zn composites goes to completion in several steps. On the basis of discussed thermal degradation profiles and $E - \alpha$ dependencies of UFC and UFC/Zn composites, Fig. 10 can be divided into various regions i.e. Fig. 10a–e for $f(\alpha)$, and Fig. 10a′–e′ for df/dT respectively. Mechanistic information about the thermal degradation processes taking place in UFC and UFC/Zn composites over long temperature ranges can be obtained by comparing Fig. 10a–e, a′–e′ with the standard $f(\alpha)$ and df/dT curves already given in Figs. 1 and 2 respectively. Figure 10a–a′ shows that the first step, ranges till 5% of conversion degree comprises dehydration of UFC and UFC/Zn composites and/or some weaker interactions present in their macromolecular structures, follows nucleation/growth phenomenon. The second step ranges between (0.05, 0.4) of 'α' is further divided into two substeps as shown in Fig. 10b–c, b′–c′ respectively. In the case of UFC, both the sub-steps obey nucleation/growth mechanisms; first one more probably is the conversion of methyl
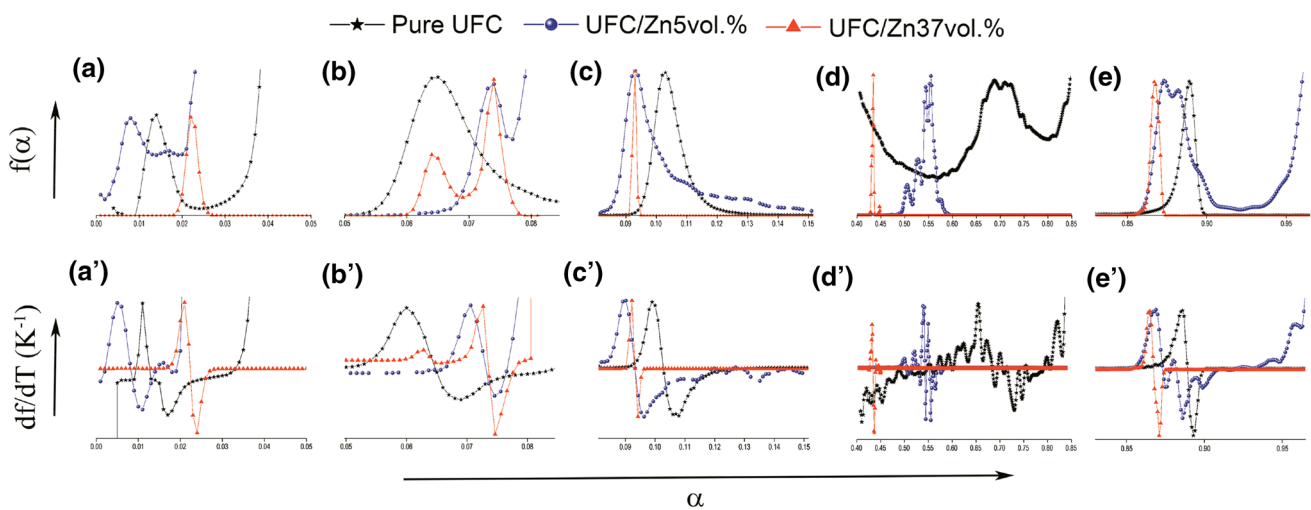

Fig. 10 **a–e** Normalized reaction models of the thermal degradation of pure UFC, UFC/Zn5vol.%, and UFC/Zn37vol.%. evaluated by advanced reaction model determination methodology at 20 °C min^{-1} and **a′–e′** Application and normalization of df/dT function on the thermal degradation of pure UFC, UFC/Zn5vol.% and UFC/Zn37vol.%. at 20 °C min^{-1}

ether groups into methylene groups, while second one could predominantly be assigned to branching/cross linking reactions taking place in UFC. Regarding UFC/Zn5vol.%, the two sub-steps follow more or less similar reaction pathways as UFC resin, though, the processes are overlapped. UFC/Zn37vol.% composite, on the other hand follows three different degradation reactions within (0.05, 0.4) range of degree of conversion. The first one is nucleation, while the rest of the two are nucleation/growth mechanisms. The third degradation step corresponds to [0.45, 0.8] of 'α' and is shown in Fig. 10d–d′. As already discussed in the previous sections, this step is considerably complex, consisting of various parallel reactions. Figure 10d–d′ evidences the higher reaction complexity of UFC and UFC/Zn5vol.% composite in the third reaction step. Interestingly, UFC/Zn37vol.% composite merely shows two nucleation/growth pathways in the third degradation step. The last step corresponds to 'α' above 0.8, and is associated to char formation as described in Fig. 10e–e′. Figure 10e–e′ represents that char formation of UFC and UFC/Zn37vol.% composite could be considered as single step processes obeying nucleation/growth phenomena. Char formation in UFC/Zn5vol.% composite however obeys overlapped nucleation/growth and diffusion phenomena.

Mechanistic information related to thermal degradation of UFC and UFC/Zn composites obtained by evaluating f(α) and df/dT functions verifies the assumptions conjectured in the previous sections. It is evident that zinc is capable of altering the thermal degradation mechanism of UFC resin. Moreover, the insulating and conducting UFC/Zn composites degrade thermally by following significantly different reaction mechanisms.

in catalytic activity and heat capacity of zinc in UFC/Zn composites.

Thermal degradation kinetic analysis of UFC and UFC/Zn composites probes into their degradation mechanisms. Substantial variations in the activation energies of resin and its composites verify the complex nature of their thermal degradation. Thermal degradation reaction models of UFC and UFC/Zn composites with the help of their respective temperature derivatives show that majority of the degradation processes pursue complex nucleation/growth pathways. Zinc involves in the reaction by altering the reaction mechanism of UFC thermal degradation. Variation in the thermal degradation mechanism of UFC has also been remarked by varying contents of zinc in UFC/Zn composites.

The present study justifies the soundness of advanced reaction model determination methodology in fairly predicting the reactions mechanisms of complex multi-step processes. This approach to the mechanisms of condensed phase processes becomes of special interest when the exact number of reactions taking place during the thermal degradation of materials is uncertain and the true nature of reactions in regard to their mutual dependency (like UFC resin and UFC/Sn composites) is unclear. In such cases, the peak deconvolution and similar approaches are quite inadequate which advocates the applicability and inevitability of the advanced reaction model determination methodology.

The obtained results beneficially contribute in the development of economical, environmentally friendly, and multipurpose polymer composites with interesting properties for several applications.

5 Conclusion

On the basis of results and discussion, following concluding points are made:

Structural characterization of UFC and UFC/Zn composites by SEM, XRD and FTIR analyses suggests that both the resin and composites are fairly homogenous and the interactions between UFC and zinc in the composites are probably physical. Integral procedure decomposition temperature (IPDT) reveals higher thermal stabilities of UFC/Zn composites, and the increase in thermal stability of UFC has been found dependent on zinc contents.

TG/DTG analyses exhibit considerably complicated reaction profiles of UFC and UFC/Zn composites which consist of various parallel/consecutive reactions. It has been pointed out that the thermal degradation behaviors of UFC/Zn composites can be fairly explained on the basis of structure and individual thermal degradation behavior of UFC, and competitive temperature dependent variations

References

1. R. Mihai, N. Sofian, D. Rusu, Polym. Test. **20**, 409–417 (2001)
2. M. Rusu, M. Daranga, N.M. Sofian, D.L. Rusu, Mater. Plast. **35**, 15–21 (1998)
3. B. Pradhan, S.K. Majee, S.K. Batabyal, A.J. Pal, J. Nanosci. Nanotechnol. **7**, 4534–4539 (2007)
4. N.N. Greenwood, A. Earnshaw, *Chemistry of the Elements*, 2nd edn. (Butterworth-Heinemann, Oxford, 1997)
5. G. Pinto, A. Maaroufi, J. Appl. Polym. Sci. **96**, 2011–2015 (2005)
6. M.A. Arshad, A. Maaroufi, R. Benavente, J.M. Perena, G. Pinto, Polym. Compos. **34**, 2049–2060 (2013)
7. B.P. Rand, H. Richter, *Organic Solar Cells: Fundamentals, Devices, and Upscaling*. (Taylor & Francis, Florida, 2014)
8. M.A. Arshad, A. Maaroufi, Soc. Plast. Eng. (2015). doi:10.2417/spepro.006183
9. M.A. Arshad, A. Maaroufi, R. Benavente, G. Pinto, Polym. Compos. **37**, 5–16 (2016)
10. S. Vyazovkin, *Isoconversional Kinetics of Thermally Stimulated Processes*. (Springer, New York, 2015)
11. M.A. Arshad, A. Maaroufi, J. Non-Crystalline Solids **413**, 53–58 (2015)

12. S. Vyazovkin, A.K. Burnham, J.M. Craido, L.A. Pérez-Maqueda, C. Popescu, N. Sbirrazzuoli, Thermochim. Acta **520**, 1–19 (2011)
13. M.E. Brown, P.K. Gallagher, *Handbook of Thermal Analysis and Calorimetry: Recent Advances, Techniques and Applications*. (Elsevier B.V., Amsterdam, 2008)
14. S. Vyazovkin, K. Chrissafis, M.L.D. Lorenzo, N. Koga, M. Pijolat, B. Roduit, N. Sbirrazzuoli, J.J. Sunol, Thermochim. Acta **590**, 1–23 (2014)
15. M.E. Brown, D. Dollimore, A.K. Galwey, *Comprehensive Chemical Kinetics*. (Elsevier, Amsterdam, 1980)
16. M. Fanfoni, M. Tomellini, Il Nuovo Cimento **20**, 1171–1182 (1998)
17. F. Booth, Trans. Faraday Soc. **44**, 796–801 (1948)
18. A. Khawam, D.R. Flanagan, J. Phys. Chem. B **110**, 17315–17328 (2006)
19. A.M. Ginstling, B.I. Brounshtein, J. Appl. Chem. USSR **23**, 1327–1338 (1950)
20. W.Z. Jander, Anorg. Allg. Chem. **163**, 1–30 (1927)
21. J. Sestak, G. Berggren, Thermochim. Acta **3**, 1–12 (1971)
22. P.W.M. Jacobs, F.C. Tompkins, *Chemistry of the Solid State*. (Academic Press, New York, 1955)
23. M.A. Arshad, A. Maaroufi, Thermochim. Acta **585**, 25–35 (2014)
24. J.H. Flynn, Thermochim. Acta **300**, 83–92 (1997)
25. J.H. Flynn, L.A. Wall, J. Res. Nat. Bur. Stand. A Phys. Chem. **70**(6), 487–523 (1966)
26. T. Akahira, T. Sunose, Sci. Technol. **16**, 22–31 (1971)
27. M.J. Starink, Thermochim. Acta **404**, 163–176 (2003)
28. J.M. Criado, L.A. Pérez-Maqueda, P.E. Sánchez-Jiménez, J. Therm. Anal. Calorim. **82**, 671–675 (2005)
29. S. Park, J.O. Baker, M.E. Himmel, P.E. Parilla, D.K. Johnson, Biotechnol. Biofuels **3**, 1–10 (2010)
30. E. Roumeli, E. Papadopoulou, E. Pavlidou, G. Vourlias, D. Bikiaris, K.M. Paraskevopoulos, K. Chrissafis, Thermochim. Acta **527**, 33–39 (2012)
31. I.M. Arafa, M.M. Fares, A.S. Braham, Eur. Polym. J. **40**, 1477–1487 (2004)
32. M.A. Arshad, A. Maaroufi, G. Pinto, S. El-Barkany, A. Elidrissi, Bull. Mater. Sci. **39**, 1609–1618 (2016)
33. A.K. Zak, W.H.A. Majid, M.E. Abrishami, R. Yousefi, Solid State Sci. **13**, 251–256 (2011)
34. Joint Committee on Powder Diffraction Standards, Powder Diffraction File (JCPDS-ICDD) No. 036 1451 and #00-004-0831.
35. S.S. Jada, J. Appl. Polym. Sci. **35**, 1573–1592 (1988)
36. H. Yang, R. Yan, H. Chen, D.H. Lee, C. Zheng, Fuel **86**, 1781–1788 (2007)
37. F. Xu, J.X. Sun, R. Sun, P. Fowler, M.S. Baird, Ind. Crop Prod. **23**, 180–193 (2006)
38. B.C. Smith, *Infrared Spectral Interpretation: A Systematic Approach*. (CRC Press, Boca Raton, 1998)
39. M.O. Edoga, Leonardo Elect. J. Pract. Tehnol. **9**, 63–80 (2006)
40. S. Samarzija-Jovanovic, V. Jovanovic, S. Konstantinovic, G. Markovic, M. Marinovic-Cincovic, J. Therm. Anal. Calorim. **104**, 1159–1166 (2011)
41. K. Siimer, T. Kaljuvee, P. Christjanson, I. Lasn, J. Therm. Anal. Calorim. **84**, 71–77 (2006)
42. C. Camino, C. Operti, L. Trossarelli, Polym. Degrad. Stab. **5**, 161–172 (1983)
43. S. Spoljaric, K.K. Wong, M. Pannirselvam, G.J. Griffin, R.A. Shanks, S. Setunge, Chemeca **41**, 805–811 (2013)
44. V. Malmeev, S. Bourbigot, J. Yvon, J. Anal. Appl. Pyrolysis **80**, 151–156 (2007)
45. V. Malmeev, S. Bourbigot, M.L. Bras, J. Yvon, Chem. Eng. Sci. **61**, 1276–1292 (2006)
46. M.A. Arshad, A. Maaroufi, R. Benavente, G. Pinto, J. App. Polym. Sci. **134**, 1–13 (2017)
47. M.A. Arshad, A. Maaroufi, R. Benavente, G. Pinto, J. Mater. Environ. Sci. **5**, 1342–1354 (2014)
48. M.D. Argyle, C.H. Bartholomew, Catalysts **5**, 145–269 (2015)
49. P.-Y. Kuo, L.A. Barros, Y.-C. Sheen, M. Sain, J.S.Y. Tjong, N. Yan, J. Anal. Appl. Pyrolysis **117**, 199–213 (2016)
50. W.S. Wang, H.S. Chen, Y.W. Wu, T.Y. Tsai, Y.W. Chen-Yang, Polymer **49**, 4826–4836 (2008)
51. C.D. Doyle, Anal. Chem. **33**, 77–79 (1961)